



Dynamic contrast enhanced MRI for characterization of blood-brain-barrier dysfunction after traumatic brain injury

Jeffrey B. Ware^{a,*}, Saurabh Sinha^b, Justin Morrison^c, Alexa E. Walter^c, James J. Gugger^c, Andrea L.C. Schneider^{c,d}, Cian Dabrowski^c, Hannah Zamore^c, Leroy Wesley^c, Brigid Magdamo^b, Dmitriy Petrov^b, Junghoon J. Kim^e, Ramon Diaz-Arrastia^c, Danielle K. Sandsmark^c

^a Division of Neuroradiology, Department of Radiology, Hospital of University of Pennsylvania, Perelman School of Medicine of the University of Pennsylvania, 3400 Spruce Street, Philadelphia, PA 19104, USA

^b Department of Neurosurgery, Perelman School of Medicine, University of Pennsylvania, 3400 Spruce Street, Philadelphia, PA 19104, USA

^c Department of Neurology, Perelman School of Medicine, University of Pennsylvania, 3400 Spruce Street, Philadelphia, PA 19104, USA

^d Department of Biostatistics, Epidemiology, and Informatics, Perelman School of Medicine, University of Pennsylvania, 3400 Spruce Street, Philadelphia, PA 19104, USA

^e Department of Molecular, Cellular, and Biomedical Sciences, CUNY School of Medicine at The City College of New York, Townsend Harris Hall, 160 Convent Avenue, New York, NY 10031, USA

ARTICLE INFO

Keywords:

TBI
Dynamic contrast-enhanced MRI
Blood-brain-barrier
Microvascular injury

ABSTRACT

Background and Purpose: Dysfunction of the blood-brain-barrier (BBB) is a recognized pathological consequence of traumatic brain injury (TBI) which may play an important role in chronic TBI pathophysiology. We hypothesized that BBB disruption can be detected with dynamic contrast-enhanced (DCE) MRI not only in association with focal traumatic lesions but also in normal-appearing brain tissue of TBI patients, reflecting microscopic microvascular injury. We further hypothesized that BBB integrity would improve but not completely normalize months after TBI.

Materials and Methods: DCE MRI was performed in 40 adult patients a median of 23 days after hospitalized TBI and in 21 healthy controls. DCE data was analyzed using Patlak and linear models, and derived metrics of BBB leakage including the volume transfer constant (K^{trans}) and the normalized permeability index (NPI) were compared between groups. BBB metrics were compared with focal lesion distribution as well as with contemporaneous measures of symptomatology and cognitive function in TBI patients. Finally, BBB metrics were examined longitudinally among 18 TBI patients who returned for a second MRI a median of 204 days postinjury. **Results:** TBI patients exhibited higher mean K^{trans} ($p = 0.0028$) and proportion of suprathreshold NPI voxels ($p = 0.001$) relative to controls. Tissue-based analysis confirmed greatest TBI-related BBB disruption in association with focal lesions, however elevated K^{trans} was also observed in perilesional ($p = 0.011$) and nonlesional ($p = 0.044$) regions. BBB disruption showed inverse correlation with quality of life ($\rho = -0.51$, corrected $p = 0.016$). Among the subset of TBI patients who underwent a second MRI several months after the initial evaluation, metrics of BBB disruption did not differ significantly at the group level, though variable longitudinal changes were observed at the individual subject level.

Conclusions: This pilot investigation suggests that TBI-related BBB disruption is detectable in the early post-injury period in association with focal and diffuse brain injury.

1. Introduction

Traumatic brain injury (TBI) is a known risk factor for the development of late-life neurodegenerative disease (Zlokovic, 2011). While the

factors driving trauma-related neurodegeneration (TReND) (Smith et al., 2019) are incompletely understood, microvascular injury and in particular blood brain barrier (BBB) dysfunction are recognized pathological consequences of TBI (Hay et al., 2015) representing potential

Abbreviations: TBI, Traumatic brain injury; DCE, dynamic contrast-enhanced; BBB, blood-brain-barrier.

* Corresponding author.

E-mail address: jeffrey.ware2@pennteam.upenn.edu (J.B. Ware).

<https://doi.org/10.1016/j.nicl.2022.103236>

Received 9 June 2022; Received in revised form 30 September 2022; Accepted 16 October 2022

Available online 17 October 2022

2213-1582/© 2022 The Authors. Published by Elsevier Inc. This is an open access article under the CC BY-NC-ND license (<http://creativecommons.org/licenses/by-nc-nd/4.0/>).

mechanisms of secondary, slowly progressive brain tissue damage following the initial impact. Chronic neurotoxicity resulting from the inability of endothelial cells and pericytes to limit the entry of plasma-derived proteins, circulating metals, and inflammatory cells into the brain is increasingly recognized in the pathogenesis of several neurodegenerative disorders including Alzheimer Disease (AD) and other AD-related dementias (ADRDs) (Zlokovic, 2011). Thus, there is a strong rationale to determine how BBB dysfunction after TBI may underpin the development of poor long-term cognitive outcomes after TBI as well as TReND (Smith et al., 2019).

TBI-related BBB breakdown is readily detectable radiologically in association with traumatic contusions in the early post-injury period manifested by parenchymal hemorrhage, vasogenic edema, and contrast-enhancement (Kushi et al., 1994; Schweitzer et al., 2019). Pathological and experimental studies also indicate that more subtle and widespread TBI-related BBB dysfunction is frequently present beyond the extent of focal anatomical lesions or hemorrhage, and may persist well into the chronic postinjury phase (Hay et al., 2015; Johnson et al., 2018). This lower-level, chronic elevation in BBB permeability, while occult on conventional neuroimaging sequences, is potentially detectable with dynamic contrast enhanced (DCE) MRI, which quantifies temporal enhancement properties driven by the movement of low-molecular weight MRI contrast agents from the vascular compartment to the extravascular extracellular space. While DCE has most frequently been used for assessing microvascular pathology associated with tumors in neuro-oncologic applications, it has also proven useful in characterizing lower-level BBB dysfunction associated with aging, neurovascular, and neuroinflammatory conditions when contrast enhancement is not visibly apparent (Montagne et al., 2015; Chi et al.; Li et al., 2018).

The ability of neuroimaging to detect and characterize frank BBB disruption as well as more subtle BBB leakage therefore holds potential to reveal the natural history of BBB dysfunction after TBI and advance the understanding of the mechanisms driving TReND. This may in turn allow for the development of novel biomarkers for improved patient prognostication, and ultimately reveal new avenues for therapeutic intervention to mitigate progressive neurological deterioration after TBI. Initial investigations of DCE MRI in TBI have suggested that BBB dysfunction is detectable in individuals exposed to repetitive sub-concussive head trauma (Weissberg et al., 2014) and mild TBI (Yoo et al., 2019), and is correlated with serologic markers of BBB damage, providing validation of DCE findings. Nevertheless, there are many unknowns about the frequency and extent of BBB dysfunction after TBI, relationship to focal lesions, and evolution over time. Furthermore, as recent evidence suggests that different approaches to DCE MRI analysis shed light on different mechanisms of BBB leakage (Veksler et al., 2020), we aimed in this preliminary study to characterize patterns of fast and slow contrast leakage in the early post-TBI period and assess their persistence over time.

2. Materials and methods

2.1. Subjects

This study was approved by the Institutional Review Board of the University of Pennsylvania and written informed consent was provided by each participant or their legally authorized representative. Each participant or their representative was informed of the potential for gadolinium retention from the contrast administration as part of the informed consent process. Adult patients with TBI, as defined by the Department of Defense (Management of Concussion/mTBI Working Group, 2009), and were hospitalized (either due to TBI or for other concurrent injuries) were enrolled at the time of hospital admission. Patients were excluded if they had a history of pre-existing serious neurological or psychiatric disease as determined by study personnel, comorbid disabling condition limiting outcome assessment, current pregnancy, or were incarcerated. Healthy control subjects with similar

demographics to the TBI patient population were also recruited and were included if they had no history of TBI within the previous 1 year, pre-existing disabling neurological or psychiatric disorders, or current pregnancy.

From an initial cohort of 46 TBI patients and 22 control participants, 6 TBI patients and 1 control participant were excluded due to poor quality DCE data (insufficient volumes acquired, insufficient pre-contrast volumes, or severely degraded by artifacts). TBI patients were imaged at a median of 23 days (range 8–79 days) post-injury. A subset of 18 TBI patients returned for a second MRI at a median of 204 days (range 166–317 days) post-injury, at which time they were also screened for additional head injuries sustained during the follow-up interval. Control subjects underwent a single MRI examination.

Demographic information, medical history, injury characteristics, and other clinical information were collected from the medical record and personal interview. Injury characteristics included the post-resuscitation Glasgow Coma Scale (GCS) score, presence or absence of loss of consciousness (LOC), and presence or absence of acute TBI-related intracranial findings on the initial head CT. Neuropsychological tests were administered within 21 days of the MRI and included the Controlled Oral Word Association Test (COWAT) (Benton et al., 1994), Rey Auditory Verbal Learning Test (RAVLT) for immediate recall (Lezak et al., 2004), Trail-Making-Test parts A and B (TMT-A/B) (Reitan et al., 1985), and the Processing Speed Index (PSI) from the Wechsler Adult Intelligence Scale-IV (WAIS) (Wechsler, 2014). Post-TBI symptoms were assessed with the Rivermead Post-Concussion Symptom Questionnaire (RPQ) (King et al., 1995), Satisfaction with Life Scale (SWLS) (McMahon et al., 2014), and Brief Symptom Inventory-18 (BSI-18). Global functional outcome was assessed using the Glasgow Outcome Scale-Extended (GOS-E) (Jennett et al., 1981).

2.2. Imaging

Brain MRIs were performed on a 3 T scanner (Siemens Prisma) using a product 32-channel head coil. Structural imaging included a sagittal T1-weighted MPRAGE (TR = 2.3 s, TE = 2.94 ms, TI = 900 ms, FA = 9°, resolution = 1 × 1 × 1 mm) as well as a sagittal 3-D FLAIR (TR = 6 s, TE = 390 ms, TI = 2100 ms, FA = 120°, resolution = 1.2 × 0.5 × 0.5 mm). Whole brain DCE imaging was performed using an axial 3D fast-spoiled gradient echo-recalled T1-weighted sequence (TR = 2 ms, TE = 4 ms, FA = 15°, FOV = 24 cm, slice thickness = 6 mm, matrix = 256 × 256) prior to (3–4 pre-contrast volumes) and after gadolinium-containing intravenous contrast administration at standard clinical dose (0.1 mmol/kg) (either gadobenate dimeglumine or gadoterate meglumine) via power injection. Whole brain DCE images were acquired at a temporal resolution of 18 s for a total scan duration of 15 min. Prior to the dynamic series, whole brain images were acquired across three flip angles (5°, 15°, 25°) with otherwise identical parameters.

2.3. Image analysis

Structural (T1 and FLAIR) images were used for manual segmentation of focal lesions by a neurosurgery resident (S.S.), which were verified and edited as needed by a neuroradiologist (J.W.). Focal lesions were defined as consisting of any parenchymal signal changes determined to represent hemorrhage, contusion, vasogenic edema, or encephalomalacia. The perilesional region was defined as all normal-appearing brain tissue within 10 mm of the focal lesion. Structural image processing was subsequently performed using the Advanced Normalization Tools (ANTs) software package (Avants et al., 2011), which included bias correction, creation of a brain mask, and 6-tissue segmentation. A population-specific anatomical template was created from 20 TBI patients and 20 control subjects selected at random, and T1-weighted images were normalized to the template using the ANTs symmetrical diffeomorphic registration tool (SyN) with B-spline interpolation (Avants et al., 2008). When present, focal lesions were used in

constraining the cost function mask to improve registration accuracy (Andersen et al., 2010; Ripollés et al., 2012).

DCE images were motion-corrected using the tools available in FSL (Jenkinson et al., 2012) and the mean of the corrected DCE timeseries was used to co-register the DCE data with the high resolution structural scan using an affine transformation computed in ANTs (Avants et al., 2008). The resultant inverse registration was then used to transform the structural brain mask into the DCE data space and remove non-brain tissue. Whole-brain T1 maps were created from the variable flip angle images and were used to transform voxel-wise DCE signal intensity data into contrast concentrations using the relaxivity of the contrast material used in each subject. For quantitative analysis, brain masks were eroded by 2 voxels to prevent contamination by high values occurring in the meninges and blood vessels just beyond the edge of the brain.

Contrast concentration timeseries data were then analyzed using two methods. First, data were fit to the Patlak model (Patlak et al., 1983) as implemented in the ROCKETSHIP (Barnes et al., 2015) software package, using automated extraction of the vascular input function (VIF) from within a mask drawn over the superior sagittal sinus in each subject. Voxel-wise maps of the volume transfer constant (K^{trans}), which approximates the permeability surface-area product (PS) under conditions of high flow and low rate of contrast extravasation (Sourbron and Buckley, 2013) were used for subsequent analyses, expressed in units of $1 \times 10^{-4} \text{ min}^{-1}$ assuming a brain tissue density of 1 g/mL. To reduce the impact of noise which disproportionately impacts the extreme low end of K^{trans} distribution (van de Haar et al., 2017), calculated values below $0.1 \times 10^{-4} \text{ min}^{-1}$ were excluded from the analysis. Second, voxel-wise DCE data were used for linear dynamic permeability analysis (Chassidim et al., 2013) in which a linear fit is applied to the slope of the later portion of the contrast concentration curve (6–15 min post-injection) normalized to that of the superior sagittal sinus yielding whole brain maps of the normalized permeability index (NPI).

2.4. Statistical analysis

All statistical analysis was performed in R (version 4.1.2). Demographic characteristics were compared between TBI and control groups using t-tests for continuous measures and Fisher’s exact test for categorical measures. DCE data was first analyzed in each subject’s DCE imaging space, where mean K^{trans} and NPI values were averaged across the brain (cerebral cortex, white matter, brainstem, and deep grey structures). Furthermore, the extent of elevated BBB permeability in each subject was computed, defined as the proportion of brain tissue voxels exhibiting K^{trans} and NPI values above the 95th percentile value of the control population. These metrics were compared between the control and subacute TBI groups using the nonparametric Mann-Whitney-U test due to the non-normal distribution of these variables. Next, tissue-based analysis was performed in the space of each subacute TBI patient’s T1-weighted structural image. Mean K^{trans} and NPI values were compared between focal lesions, perilesional tissue, and normal-appearing brain tissue using paired Wilcoxon signed-rank tests. To gain insight into the spatial distribution of BBB disruption in the TBI group, a threshold-weighted K^{trans} overlap map was created in template space using a previously described procedure (Seghier and Price, 2016) which quantifies the proportion of subjects showing elevated permeability at each brain voxel unbeholden to a single arbitrary threshold. Furthermore, overlap of suprathreshold NPI voxels was also computed in the template space. Next, DCE measures exhibiting the largest differences between TBI and control participants were compared with injury characteristics and clinical measures among the TBI group using Spearman’s rank correlation, with p values corrected for multiple comparisons using the false discovery rate (FDR) method. For comparison with outcome, the TBI group was dichotomized based on the GOS-E score into “less disabled” ($\text{GOS-E} \geq 7$; near or complete return to pre-injury baseline function) and “more disabled” ($\text{GOS-E} < 7$; not returned to pre-injury baseline function) outcome groups. The extent of

elevated BBB was compared between outcome groups using the Mann-Whitney-U test. The extent of BBB permeability elevation was examined longitudinally within the subgroup of TBI patients who returned for follow-up scanning using the Wilcoxon signed-rank test for paired samples. Lastly, to investigate the possibility that results may be driven by the few patients with moderate or severe TBI ($\text{GCS} < 13$), a sensitivity analysis was performed in which the above-described analyses were repeated with these subjects excluded.

3. Results

1%1 Demographic characteristics of the study population are displayed in Table 1. TBI and controls showed no statistically significant group differences in age, sex, or education level. Among the TBI group, 29 (72.5 %) experienced confirmed or suspected loss of consciousness, 22 (55 %) had a trauma-related intracranial abnormality on the initial head CT, and 17 (42.5 %) were found to have a focal TBI-related brain parenchymal lesion on MRI. An example lesion segmentation in a representative patient with a right occipital hemorrhagic contusion along with contrast concentration curves stratified by tissue type is displayed in Fig. 1. While the median GOS-E of TBI group was 7, 46 % of TBI patients had a “more disabled” outcome ($\text{GOS-E} < 7$), and a subset had

Table 1
Demographic characteristics of the TBI and control groups, and injury characteristics of the TBI group.

	Control (N = 21)	TBI (N = 40)	p value
Age (years)			
Mean (SD)	33.8 (11.8)	35.5 (14.5)	0.626
Median [Min, Max]	32.0 [20.0, 59.0]	30.5 [18.0, 68.0]	
Sex			
Male	11 (52.4 %)	30 (75.0 %)	0.0909
Female	10 (47.6 %)	10 (25.0 %)	
Race			
White	10 (47.6 %)	13 (32.5 %)	0.0166
Black	6 (28.6 %)	25 (62.5 %)	
Other	5 (23.8 %)	2 (5.0 %)	
Education Level			
Beyond High School	13 (61.9 %)	21 (52.5 %)	0.271
High School or Equivalent	2 (9.5 %)	9 (22.5 %)	
Less than High School	0 (0 %)	3 (7.5 %)	
Missing	6 (28.6 %)	7 (17.5 %)	
Positive CT			
Yes	–	22 (45.0 %)	–
No	–	18 (55.0 %)	
Glasgow Coma Scale (GCS)			
Median [25th percentile, 75th percentile]	–	15.0 [14, 15]	–
Range	–	3–15	
Missing	–	2 (5.0 %)	
GCS Category			
Mild	–	34 (85.0 %)	–
Moderate	–	3 (7.5 %)	
Severe	–	1 (2.5 %)	
Missing	–	2 (5.0 %)	
Loss of Consciousness			
Yes (or suspected)	–	29 (72.5 %)	–
No	–	6 (15.0 %)	
Missing	–	5 (12.5 %)	
Post-Traumatic Amnesia			
Yes (or suspected)	–	21 (52.5 %)	–
No	–	9 (22.5 %)	
Missing	–	10 (25.0 %)	
Injury Mechanism			
Road Traffic Incident	–	25 (62.5 %)	–
Fall	–	7 (17.5 %)	
Other (Non-Intentional Injury, Assault)	–	6 (15.0 %)	
Missing	–	2 (5.0 %)	

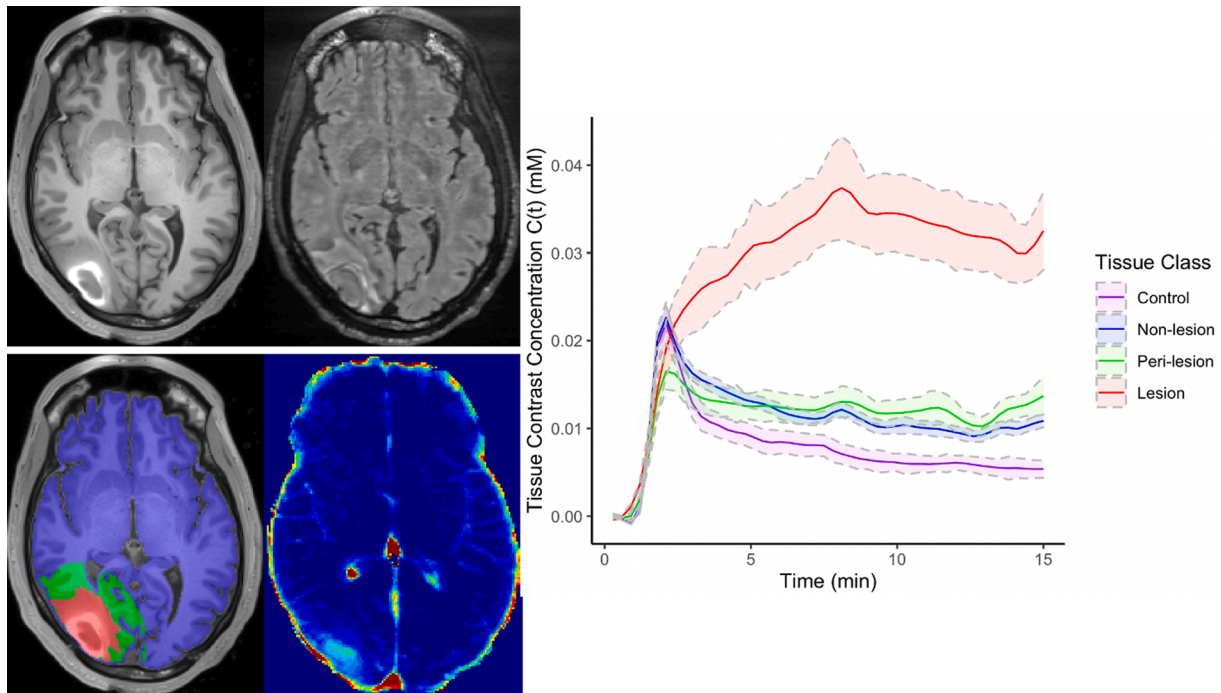


Fig. 1. T1 (top left) and FLAIR (top right) images depict a right occipital lobe hemorrhagic contusion with surrounding edema in a TBI patient, with the corresponding tissue segmentation result (bottom left). The contrast concentration map from a single DCE timepoint demonstrates contrast accumulation in the contusion (bottom right). Corresponding contrast concentration curves are shown on the right, with an aligned and superimposed curve from a control subject.

persistent posttraumatic symptoms with TBI patients exhibiting a median RPQ score of 14.5 (IRQ 15.74) and a median SWLS score of 25 (IQR 11).

2% Representative subject DCE examples are displayed in Fig. 2, demonstrating that elevations in BBB permeability are observable in some TBI patients without focal lesions. Group-wise comparisons demonstrated higher mean K^{trans} ($W = 226, p = 0.0028,$

Fig. 3A) as well as a greater proportion of suprathreshold K^{trans} voxels ($W = 259, p = 0.013,$ Fig. 3C) among the subacute TBI group compared to the control group. Mean brain NPI was higher in the TBI group though the difference did not reach statistical significance ($W = 315, p = 0.11,$ Fig. 3B). The proportion of suprathreshold NPI voxels was significantly higher among the TBI group compared to the control group ($W = 204, p = 0.001,$

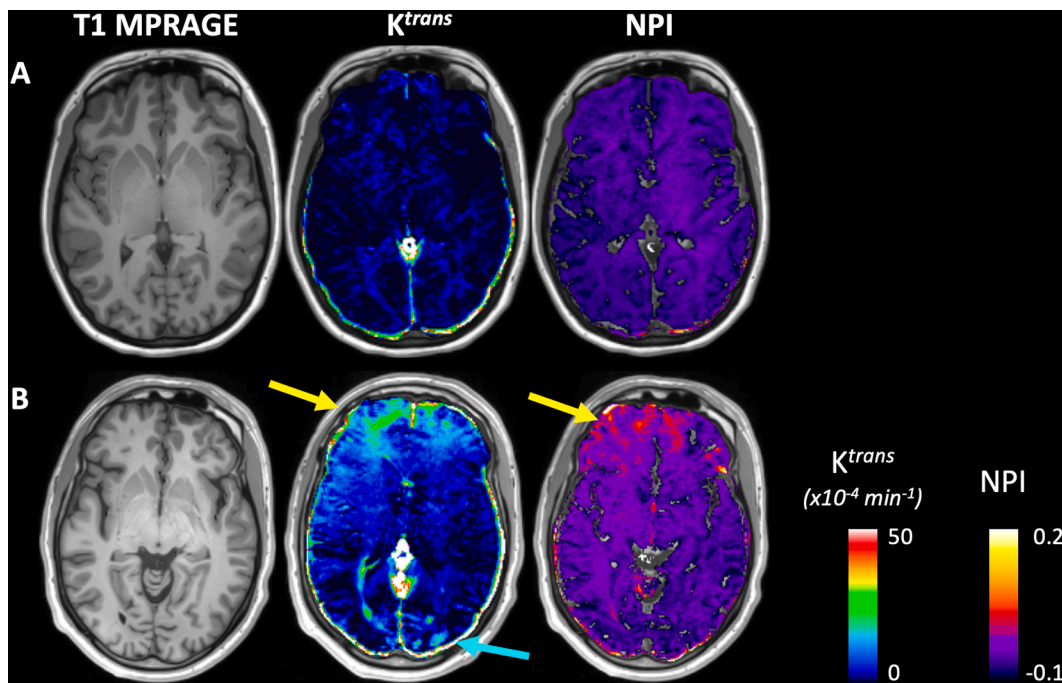


Fig. 2. Individual subject examples from a representative control (A) and subacute TBI subject (B). The TBI nonlesional patient shows similar mild elevations in K^{trans} and NPI in the anterior frontal white matter (yellow arrows), and additional small areas of K^{trans} elevation in the occipital lobes (blue arrow). (For interpretation of the references to colour in this figure legend, the reader is referred to the web version of this article.)

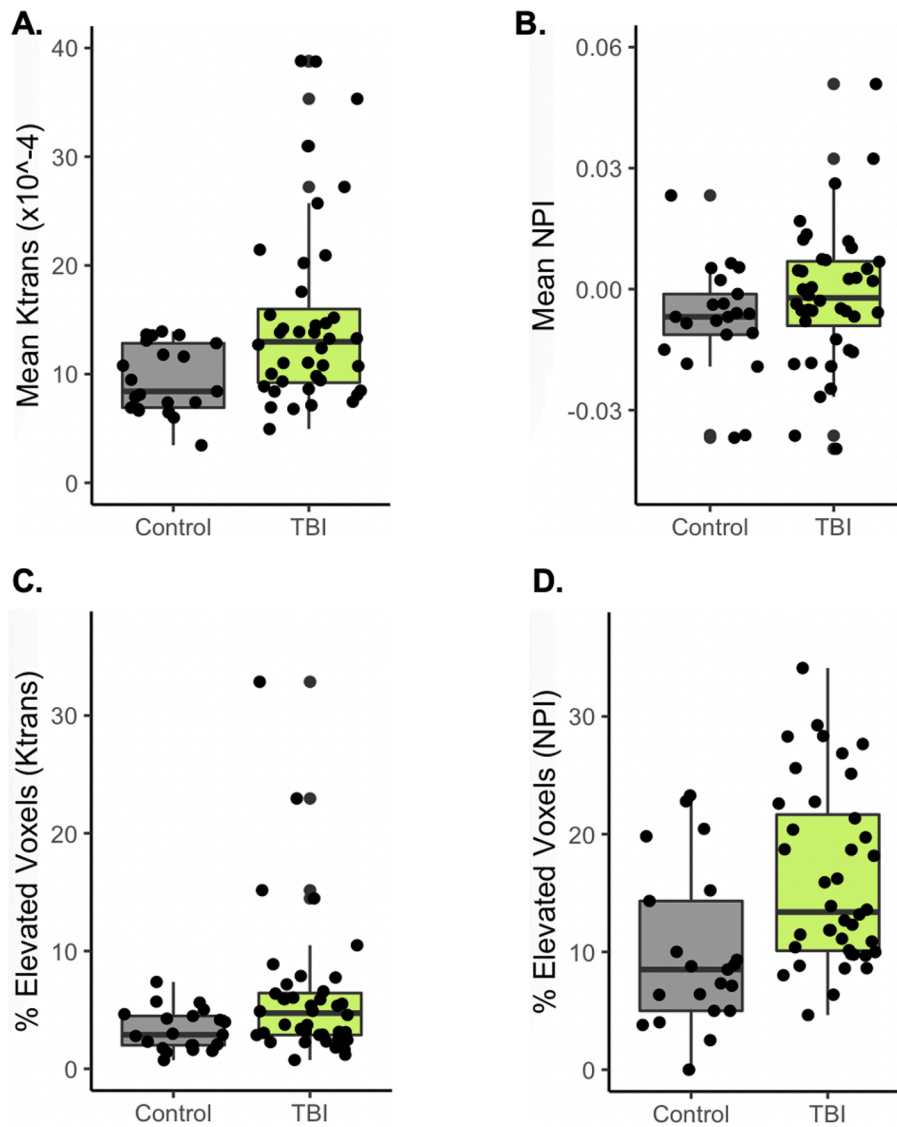


Fig. 3. Group-level comparisons between the subacute TBI and control groups demonstrate elevated mean K^{trans} (A, $p = 0.0028$) and a greater proportion of voxels exceeding the control group 95th percentile K^{trans} value (B, $p = 0.014$) among the TBI group. There was no statistically significant difference in mean NPI between groups (C, $p = 0.11$), however there was a greater proportion of voxels exceeding the control group 95th percentile NPI value (D, $p = 0.001$) among the TBI group.

Fig. 3D). Threshold-weighted overlap maps created from K^{trans} data among the TBI group (Fig. 4C) demonstrated a spatial distribution of elevated permeability which resembled that of focal lesions (Fig. 4A), however there were areas with elevated permeability where no lesions were present such as in the anterior frontal lobes more superiorly, and in general showing a predilection for peripheral aspects of the brain. An overlap map of suprathreshold NPI voxels in the TBI group (Fig. 4D) showed a similar pattern of elevated permeability also resembling the distribution of focal lesions, however there were some areas where permeability elevation appeared more expansive than with K^{trans} such as in the high anterior frontal white matter. Tissue-based analysis confirmed highest K^{trans} and NPI values within focal traumatic lesions ($p < 0.001$ for both). K^{trans} was elevated to a lesser degree in the perilesional ($p = 0.011$) and across nonlesional ($p = 0.044$) regions in comparison to the control group (Fig. 5A). NPI was also elevated in the perilesional region ($p = 0.004$), but not significantly elevated in nonlesional tissue (Fig. 5B, $p = 0.6$).

3%1 Subsequent analysis focused on the mean K^{trans} and the proportion of suprathreshold NPI voxels. BBB permeability metrics were

not significantly correlated with GCS ($\rho = -0.16$, $p = 0.34$ for mean K^{trans} and $\rho = 0.12$, $p = 0.48$ for suprathreshold NPI voxels). In exploratory correlation analysis with measures of clinical symptomatology and neuropsychological function (Table 2), there were moderate inverse correlations between both metrics and SWLS scores ($\rho = -0.51$, corrected $p = 0.016$ for mean K^{trans} and $\rho = -0.47$, corrected $p = 0.048$ for suprathreshold NPI voxels). A weak inverse correlation was observed between mean K^{trans} and RAVLT which was not statistically significant after multiple comparison correction ($\rho = -0.35$, corrected $p = 0.48$) (Fig. 6). BBB permeability metrics were not significantly correlated with other neuropsychological test and symptom scores (Table 2). Furthermore, TBI patients with “less disabled” and “more disabled” outcome (GOS-E ≥ 7 compared with GOS-E < 7) did not show significant differences in BBB metrics mean K^{trans} ($W = 183$, $p = 0.94$) and proportion of suprathreshold NPI voxels ($W = 200$, $p = 0.57$).

4%1 In longitudinal analysis, there were no significant differences in demographics, injury characteristics, measures of post-concussive symptoms, or outcome between TBI patients who completed the follow up scan and those who did not (Table 3).

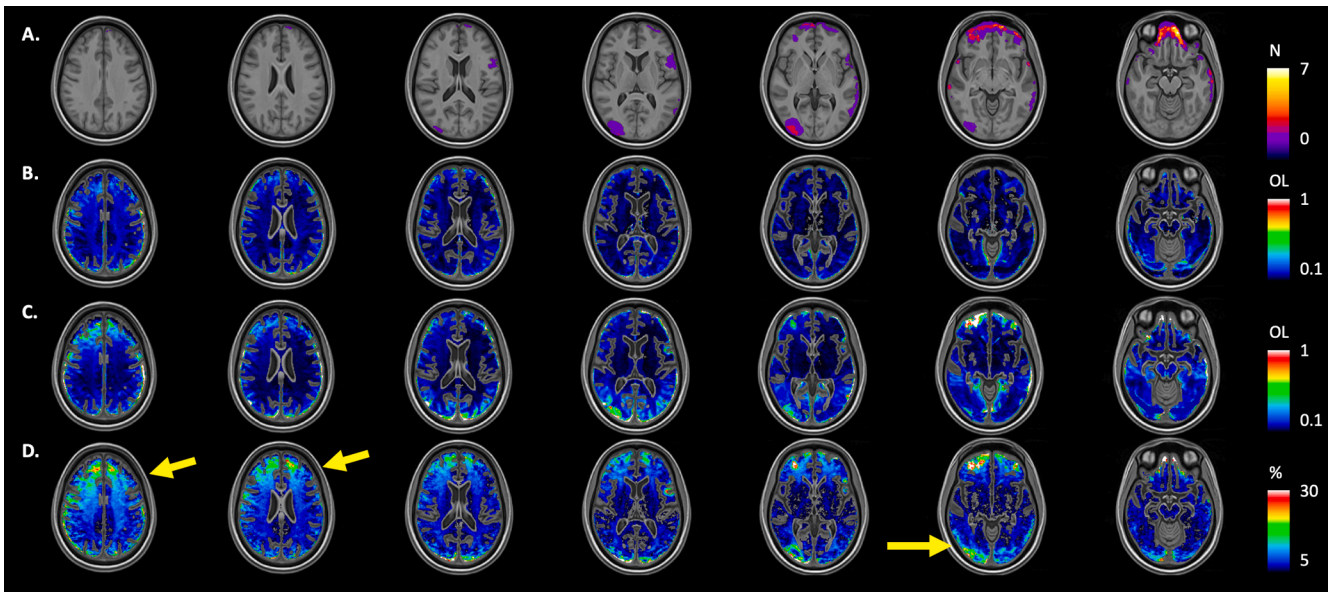


Fig. 4. Focal traumatic lesions presented as an overlap map (A) exhibited an expected predilection for anteroinferior frontal and temporal lobes, noting 2 patients had right occipital lesions. Threshold-weighted overlap maps displayed on an arbitrary scale in both control (B, provided for reference) and TBI (C) subjects demonstrate TBI-related K^{trans} elevation in a pattern resembling focal lesions but to a small degree in areas outside of lesioned brain, such as the left temporal-occipital region and high anterior frontal lobes. An overlap map of supratherreshold NPI voxels in the TBI group (D) showed a similar pattern of elevated permeability compared to K^{trans} again matching the distribution of focal lesions though there are some areas where permeability elevation appears more expansive such as in the high anterior frontal white matter.

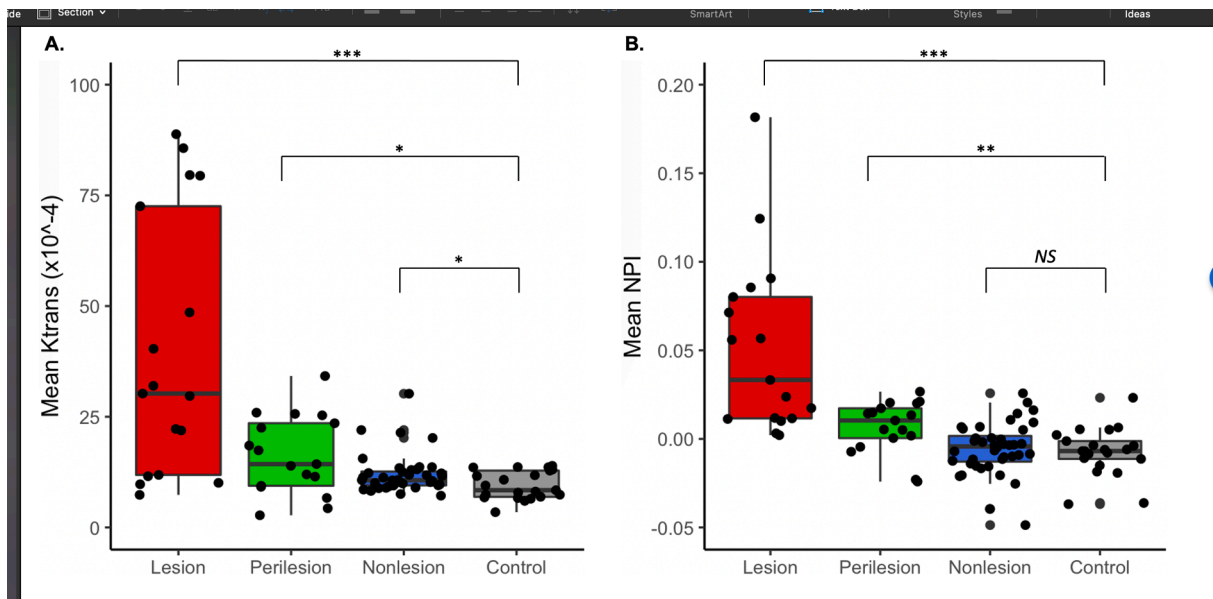


Fig. 5. Tissue-based analysis demonstrates highest K^{trans} values in association with focal lesions ($p < 0.001$), with lower but still elevated K^{trans} values in the perilesional ($p = 0.011$) and nonlesional ($p = 0.044$) regions in comparison to the control group. NPI values were similarly most elevated in focal traumatic lesions ($p < 0.001$), and to a lesser degree in the perilesional region ($p = 0.011$). NPI in the nonlesional region was not significantly different than the control group ($p = 0.6$). (***) $p < 0.001$, (**) $p < 0.01$, (*) $p < 0.05$.

Among the follow-up group, there was a decline in mean K^{trans} (average delta $-2.29 \pm 7.9 \times 10^{-4} \text{ min}^{-1}$) and proportion of supratherreshold NPI voxels (average delta $-0.9 \pm 11 \%$) at the time of follow-up across the TBI group, though which was not statistically significant in paired testing ($V = 105$, $p = 0.42$ and $V = 104$, $p = 0.44$ respectively). Decline in BBB metrics over time was greater in lesional patients (delta $K^{trans} -5.32 \pm 8.2 \times 10^{-4} \text{ min}^{-1}$ and delta NPI supratherreshold voxels $-5.1 \pm 7.2 \%$) compared to nonlesional patients (delta $K^{trans} 1.5 \pm 5.9 \times 10^{-4}$

min^{-1} and delta NPI supratherreshold voxels $6.8 \pm 12.8 \%$). Inspection of individual trajectories (Fig. 7) showed while some patients with the highest values at the initial scan (due to larger focal lesions) exhibited the largest decreases by the follow-up scan, some were relatively stable while others showed an increase. Trajectories appeared more heterogeneous with the supratherreshold NPI voxel metric than with the mean K^{trans} . In particular, three nonlesional patients (each with a GCS of 15) with lower NPI measures at the initial timepoint showed clear

Table 2

Correlation analysis between clinical measures and the extent of elevated BBB permeability as assessed by K^{trans} (third column) and NPI (fourth column) in the TBI group. * Denotes measures with statistically significant ($p < 0.05$) correlation to imaging metrics.

Measures	N	K^{trans}		NPI	
		Rho	p	Rho	p
Behavioral Rating Scales:					
RPQ	38	0.03	0.84	-0.04	0.8
SWLS*	37	-0.51	0.001	-0.47	0.003
BSI-18	37	0.18	0.29	-0.06	0.71
Neuropsychological Tests:					
PSI	35	-0.25	0.14	-0.33	0.056
COWAT	32	-0.12	0.5	0.15	0.43
RAVLT*	36	-0.35	0.03	-0.2	0.24
TMT-A	36	-0.08	0.63	-0.02	0.91
TMT-B	36	0.15	0.29	0.04	0.8

Key: RPQ – Rivermead Post Concussion Symptoms Questionnaire, SWLS – Satisfaction with Life Scale, BSI-18 – Brief Symptom Inventory-18, PSI – Processing Speed Index, COWAT – Controlled Oral Word Association Test, RAVLT – Rey Auditory Verbal Learning Test, TMT – Trail Making Test (parts A/B).

increase by the follow-up timepoint (Fig. 7). Representative individual-subject longitudinal examples are displayed in Fig. 8, including one nonlesional TBI patient who exhibited a multifocal increase in suprathreshold NPI voxels at follow-up.

5% Sensitivity analysis after excluding 4 TBI patients with GCS < 13 did not alter the primary results of statistically significant control-TBI group DCE metric differences, tissue-based DCE metric differences, and correlations between DCE metrics and a few of the clinical measures. None of the patients with GCS < 13 returned for the follow-up scan, therefore longitudinal analysis results were unaffected.

4. Discussion

This study examining patients with mild-moderate TBI in the subacute post-injury timeframe adds to the emerging literature supporting the use of DCE MRI for the detection and characterization of BBB disruption after TBI. While we observed BBB permeability was most strikingly elevated in association with focal traumatic lesions, elevation of BBB permeability was also detected in otherwise normal-appearing brain tissue surrounding and, to some degree, remote from focal lesions. TBI-related BBB permeability elevation was most frequently observed in anterior and posterior regions of the brain in a spatial distribution resembling that of focal traumatic parenchymal lesions and consistent with anatomical vulnerability to blunt structural brain injuries (Schweitzer et al., 2019). Our current results are in general agreement with previous investigations of DCE MRI which have found that measures of BBB permeability are abnormally elevated after TBI across injury severities (O’Keefe et al., 2020), including within

otherwise radiologically normal-appearing brain tissue (O’Keefe et al., 2020; Yoen et al., 2021; Tomkins et al., 2011) where permeability elevations are on the order of what has previously been observed in other diseases featuring microvascular pathology (Huisa et al., 2015). In light of recent studies demonstrating correlations between K^{trans} values and elevated serum matrix metalloproteinases (Nichols et al., 2021) and other serologic markers of BBB damage such as S100B (O’Keefe et al., 2020) after TBI, our results provide further support that DCE abnormalities after TBI reflect loss of BBB integrity.

Our study provides new insights into the evolution of BBB pathology over time and suggests BBB pathology is persistent into the early chronic phase of TBI. Inspection of individual patient trajectories suggests considerable heterogeneity, while TBI patients with larger lesions generally exhibited a decrease in magnitude and extent of BBB disruption by around 6–7 months postinjury, there were some TBI patients showing an increase in BBB disruption. These results, while preliminary, highlight the need to investigate the natural history of BBB disruption on a larger scale to better parse this heterogeneity and ultimately understand its contribution to cumulative neuropathology.

Generally, we found that relationships between BBB disruption and contemporaneous measures of symptomatology, neuropsychological function, and short-term outcome were not strong and appeared weaker than what has previously been demonstrated for traumatic axonal injury and resultant brain network disconnection (Jolly et al., 2021). This is not surprising given the dependence of these outcomes on a range of variables which notably include injury-independent psychosocial factors particularly in patients with mild TBI (Meares et al., 2011); who comprised the majority of our sample. We did, however, observe a moderate inverse correlation between measures of BBB disruption and quality of life scores, suggesting that the magnitude and extent of BBB disruption have some relevance to early posttraumatic clinical sequelae. This is consistent with previous work demonstrating correlations between BBB disruption and measures of injury severity such as GCS (Winter et al., 2015), as well as with the number and duration of injuries (O’Keefe et al., 2020), though we are limited by the lack of a more sensitive measure of injury severity. Furthermore, while a weak inverse correlation between BBB disruption and verbal learning was not statistically significant after multiple comparison correction, this relationship has been observed previously among mild TBI patients diagnosed with post-concussive syndrome (Yoo et al., 2019), and warrants further investigation. In light of previous work indicating a relationship between early and persistent BBB damage after a neurological insult and long-term clinical outcome (Lublinsky et al., 2019), the most important clinical effects of BBB pathology after TBI may take longer to manifest than the timeframe we have examined. The relevance of BBB disruption to longer-term outcomes after TBI is further supported by its histologic detection years to decades after a TBI (Hay et al., 2015) as well as its colocalization with other late-stage pathological features of chronic traumatic encephalopathy (CTE) (Tagge et al., 2018).

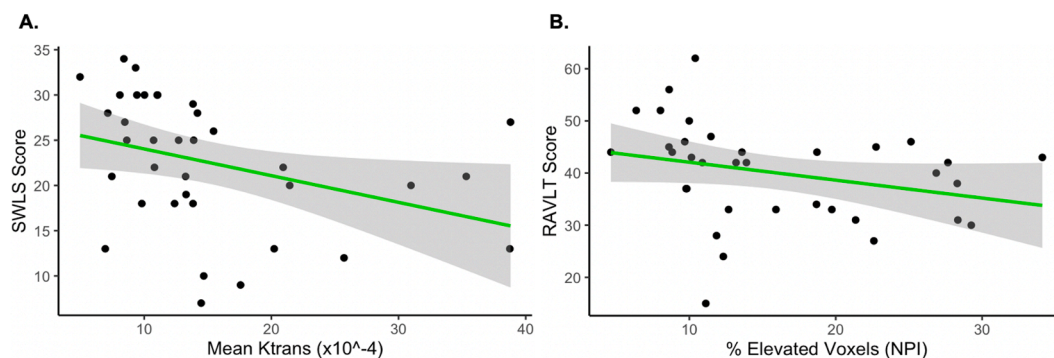


Fig. 6. Scatter plots depicting inverse correlations between the mean K^{trans} and satisfaction with life score (SWLS) (A), and between the proportion of elevated NPI voxels and RAVLT score (B).

Table 3
Demographic and clinical characteristics of the TBI group stratified by follow-up status.

	Subacute Only (N = 22)	Subacute + Follow-up (N = 18)	p value
Age (years)			
Mean (SD)	37.0 (15.5)	33.5 (13.3)	0.441
Median [Min, Max]	32.5 [18.0, 68.0]	28.5 [18.0, 64.0]	
Sex			
Male	16 (72.7 %)	14 (77.8 %)	1
Female	6 (27.3 %)	4 (22.2 %)	
Race			
White	6 (27.3 %)	7 (38.9 %)	0.569
Black	14 (63.6 %)	11 (61.1 %)	
Other	2 (9.1 %)	0 (0 %)	
Education Level			
Beyond High School	10 (45.5 %)	11 (61.1 %)	1
High School or Equivalent	5 (22.7 %)	4 (22.2 %)	
Less Than High School	1 (4.5 %)	2 (11.1 %)	
Missing	6 (27.3 %)	1 (5.6 %)	
Positive CT			
Yes	11 (50.0 %)	11 (61.1 %)	0.537
No	11 (50.0 %)	7 (38.9 %)	
Glasgow Coma Scale (GCS)			
Median [25th percentile, 75th percentile]	15.0 [14, 15]	15.0 [14, 15]	0.158
Range	3–15	13–15	
Missing	1 (4.5 %)	1 (5.6 %)	
GCS Category			
Mild	17 (77.3 %)	17 (94.4 %)	0.238
Moderate	3 (13.6 %)	0 (0 %)	
Severe	1 (4.5 %)	0 (0 %)	
Missing	1 (4.5 %)	1 (5.6 %)	
Loss of Consciousness			
Yes (or suspected)	15 (68.2 %)	14 (77.8 %)	0.207
No	5 (22.7 %)	1 (5.6 %)	
Missing	2 (9.1 %)	3 (16.7 %)	
Post-Traumatic Amnesia			
Yes (or suspected)	11 (50.0 %)	10 (55.6 %)	0.691
No	6 (27.3 %)	3 (16.7 %)	
Missing	5 (22.7 %)	5 (27.8 %)	
Injury Mechanism			
Fall	3 (13.6 %)	4 (22.2 %)	0.501
Other (Non-Intentional Injury, Assault)	2 (9.1 %)	4 (22.2 %)	
Road Traffic Incident	15 (68.2 %)	10 (55.6 %)	
Missing	2 (9.1 %)	0 (0 %)	
RPQ			
Median [Min, Max]	20 [1, 38]	14 [0, 49]	0.20
IQR	25	7	
Missing	1 (4.5 %)	1 (5.6 %)	
SWLS			
Median [Min, Max]	20.5 [7, 34]	25 [12, 34]	0.09
IQR	10.5	8	
Missing	2 (9.1 %)	1 (5.6 %)	
GOS-E			
Median [Min, Max]	7 [3, 8]	6.5 [5, 8]	0.388
IQR	2	2.75	
Missing	1 (4.5 %)	0 (0 %)	

DCE MRI is not a novel technique, however optimal methodology for quantitative BBB leakage assessment and in particular detection of low-level BBB dysfunction remains an active area of research. While highly relevant to the study of TBI as well as other neurovascular, neurodegenerative, and neuroinflammatory conditions, interstudy generalizability of low-level BBB leakage measurements have been hampered by variations in acquisition and analysis strategies. In this study we employed both the Patlak model, which has been suggested as the most suitable for detection of low-level permeability disturbances (Barnes et al., 2016; Heye et al., 2016), as well as linear dynamic analysis which may have greater sensitivity for slower mechanisms of BBB leakage (Veksler et al., 2020). We also employed a DCE acquisition duration (15

min) which, while clinically feasible, is substantially longer than typically used for clinical brain tumor imaging. In order to account for the inherent spatial heterogeneity of neuropathology expected to occur in TBI, whole brain imaging is required, necessitating compromises in spatial and temporal resolution which in turn reduce accuracy of vascular input function estimation and subsequent pharmacokinetic modeling (Raja et al., 2018). Nevertheless, we could still observe significant differences in normal-appearing brain between TBI and control participants. Encouragingly, results obtained with both methods were generally convergent, though some differences were apparent. Most notable was a longitudinal increase in BBB permeability observed in a few patients with the linear dynamic method which was not clearly apparent in K^{trans} . In the context of prior work demonstrating a correlation between linear dynamic analysis and a *trans*-cellular molecular transport mechanism across the BBB (Veksler et al., 2020), the current longitudinal results may suggest this mechanism plays a greater role in the chronic phase, at least in some patients. Nevertheless, further research into the longitudinal course of BBB disruption after TBI and validation of these results are needed before firm conclusions can be drawn.

Other limitations of this study include the small sample size, particularly for longitudinal analysis, as well as missing data from some of the TBI participants which reduced statistical power for examining neuropsychological and clinical correlates of BBB disruption. Furthermore, the use of a convenience sample which may not be entirely representative of the TBI population at large may limit the generalizability of these results, particularly the observed longitudinal trends given high rate of loss to follow-up. Variable time-from-injury for the initial and follow-up scans limits the ability to draw definitive conclusions about the time course of BBB dysfunction after TBI, but our results should encourage the undertaking of larger follow-up studies to address these issues. While concern remains over the potential for neurotoxicity related to retained gadolinium after intravenous administration of gadolinium-based contrast agents (GBCA) in patients with a compromised blood-brain barrier, research to date has not identified any associated adverse health effects, and accumulating evidence suggests that the use of macrocyclic agents minimizes deposition (Mathur et al., 2020). Ultimately the use of GBCA in research is guided by risk-benefit analysis, which in the case of TBI and related neurological conditions is informed by mounting evidence for the pathogenic role of BBB dysfunction and where improved understanding may lead to new and much needed avenues for diagnosis and therapy.

5. Conclusion

We found evidence of abnormally elevated BBB permeability within and to a lesser degree outside of focal lesions in patients with subacute TBI. These findings suggest that hospitalized TBI is associated with low-level BBB disruption in otherwise normal-appearing brain tissue which can be detected with DCE-MRI. This also encourages additional research using DCE to determine the natural history of this potentially important pathology and to better understand its contribution to long-term outcomes of chronic TBI.

Funding

This work was supported by the National Institutes of Health [Grant No R01NS125408, K23NS123340].

CRediT authorship contribution statement

Jeffrey B. Ware: Conceptualization, Methodology, Software, Formal analysis, Data curation, Writing – original draft, Writing – review & editing, Funding acquisition. **Saurabh Sinha:** Data curation, Software, Formal analysis, Writing – review & editing. **Justin Morrison:** Data curation, Investigation, Project administration. **Alexa E. Walter:** Formal

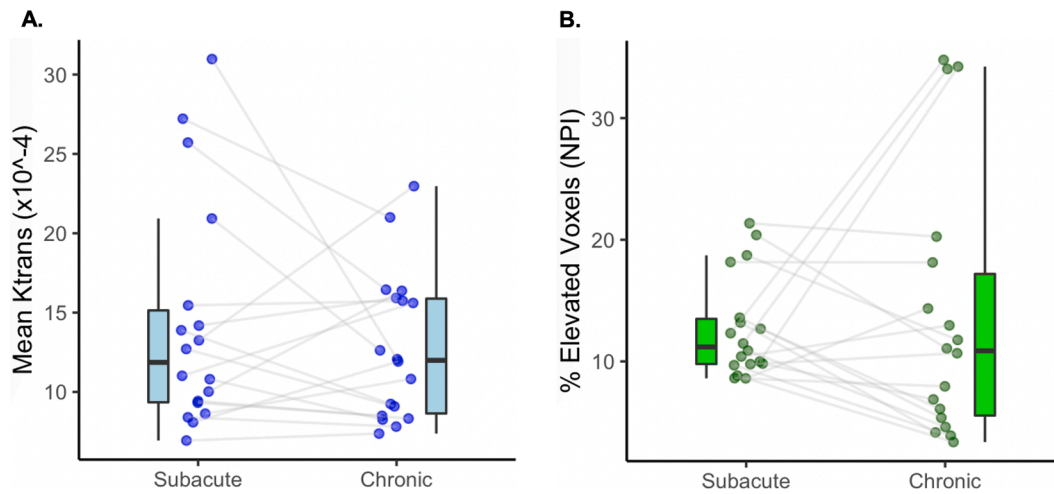


Fig. 7. Longitudinal analysis of DCE metrics among TBI patients who returned for a follow-up scan around 6 months after injury. While no significant differences were observed in these metrics between timepoints ($V = 105$, $p = 0.42$ for K^{trans} and $V = 104$, $p = 0.44$ for suprathreshold NPI voxels), individual trajectories showed considerable heterogeneity particularly in the suprathreshold NPI voxel measure.

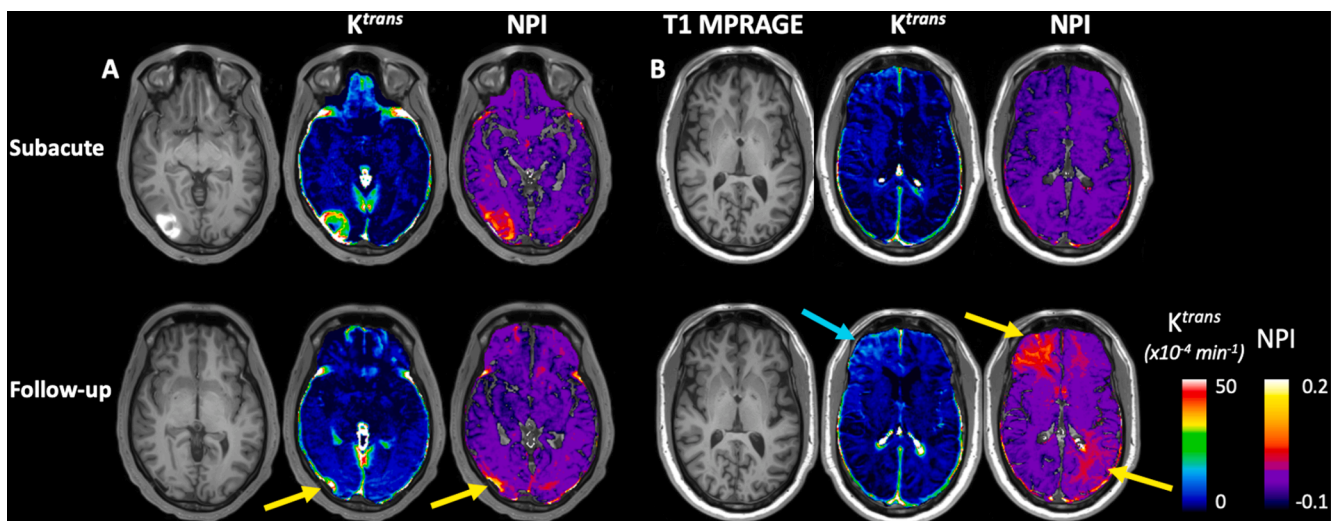


Fig. 8. Individual TBI patients examined longitudinally at the subacute (top row) and follow-up timepoints (bottom row). The patient who had a right occipital hemorrhagic contusion (GCS 15); Panel A) shows marked focal elevation in both K^{trans} and NPI at the subacute timepoint associated with the lesion. At follow-up there is a persistent but smaller area of elevated permeability in association in the same location (yellow arrows). In Panel B, the patient (GCS 15) did not have a lesion visible on structural MRI nor are there any clear BBB abnormalities at the subacute timepoint. At the time of follow-up, there were new areas of mildly elevated NPI in the right frontal and left occipital lobes (yellow arrows), present to a much lesser degree in the K^{trans} map (blue arrow). (For interpretation of the references to colour in this figure legend, the reader is referred to the web version of this article.)

analysis, Data curation, Writing – review & editing, Project administration. **James J. Gugger:** Conceptualization, Methodology, Writing – review & editing. **Andrea L.C. Schneider:** Conceptualization, Methodology, Writing – review & editing. **Cian Dabrowski:** Data curation, Investigation, Project administration. **Hannah Zamore:** Data curation, Investigation, Project administration. **Leroy Wesley:** Data curation, Validation, Investigation. **Brigid Magdamo:** Data curation, Investigation, Project administration. **Dmitriy Petrov:** Resources. **Junghoon J. Kim:** Conceptualization, Methodology, Writing – review & editing. **Ramon Diaz-Arrastia:** Conceptualization, Methodology, Resources, Writing – review & editing, Supervision, Funding acquisition. **Danielle K. Sandmark:** Conceptualization, Methodology, Writing – review & editing.

Declaration of Competing Interest

The authors declare that they have no known competing financial

interests or personal relationships that could have appeared to influence the work reported in this paper.

Data availability

Data will be made available on request.

References

- Andersen, S.M., Rapcsak, S.Z., Beeson, P.M., 2010. Cost function masking during normalization of brains with focal lesions: still a necessity? *Neuroimage* 53, 78–84.
- Avants, B.B., Epstein, C.L., Grossman, M., et al., 2008. Symmetric diffeomorphic image registration with cross-correlation: evaluating automated labeling of elderly and neurodegenerative brain. *Med. Image Anal.* 12, 26–41.
- Avants, B.B., Tustison, N.J., Song, G., et al., 2011. A reproducible evaluation of ANTs similarity metric performance in brain image registration. *Neuroimage* 54, 2033–2044.

- Barnes, S.R., Ng, T.S.C., Santa-Maria, N., et al., 2015. ROCKETSHIP: a flexible and modular software tool for the planning, processing and analysis of dynamic MRI studies. *BMC Med. Imaging* 15.
- Barnes, S.R., Ng, T.S.C., Montagne, A., et al., 2016. Optimal acquisition and modeling parameters for accurate assessment of low Ktrans blood-brain barrier permeability using dynamic contrast-enhanced MRI. *Magn. Reson. Med.* 75, 1967–1977.
- Benton AL, Hamsher K deS, Sivan AB. *Multilingual Aphasia Examination (3rd Ed.)*. Iowa City, IA: AJA Associates; 1994.
- Chassidim, Y., Veksler, R., Lublinsky, S., et al., 2013. Quantitative imaging assessment of blood-brain barrier permeability in humans. *Fluids Barriers CNS* 10, 9.
- Chi JM, Mackay M, Hoang A, et al. Alterations in Blood-Brain Barrier Permeability in Patients with Systemic Lupus Erythematosus. *AJNR Am J Neuroradiol* <https://doi.org/10.3174/ajnr.A5990>.
- Hay, J.R., Johnson, V.E., Young, A.M.H., et al., 2015. Blood-brain barrier disruption is an early event that may persist for many years after traumatic brain injury in humans. *J. Neuropathol. Exp. Neurol.* 74, 1147–1157.
- Heye, A.K., Thrippleton, M.J., Armitage, P.A., et al., 2016. Tracer kinetic modelling for DCE-MRI quantification of subtle blood-brain barrier permeability. *NeuroImage* 125, 446–455.
- Huisa, B.N., Caprihan, A., Thompson, J., et al., 2015. Long-term blood-brain barrier permeability changes in binswanger disease. *Stroke* 46, 2413–2418.
- Jenkinson, M., Beckmann, C.F., Behrens, T.E.J., et al., 2012. FSL. *Neuroimage* 62, 782–790.
- Jennett, B., Snoek, J., Bond, M.R., et al., 1981. Disability after severe head injury: observations on the use of the Glasgow Outcome Scale. *J. Neurol. Neurosurg. Psychiatry* 44, 285–293.
- Johnson, V.E., Weber, M.T., Xiao, R., et al., 2018. Mechanical disruption of the blood-brain barrier following experimental concussion. *Acta Neuropathol.* 135, 711–726.
- Jolly, A.E., Bălăeț, M., Azor, A., et al., 2021. Detecting axonal injury in individual patients after traumatic brain injury. *Brain* 144, 92–113.
- King, N.S., Crawford, S., Wenden, F.J., et al., 1995. The Rivermead Post Concussion Symptoms Questionnaire: a measure of symptoms commonly experienced after head injury and its reliability. *J. Neurol.* 242, 587–592.
- Kushi, H., Katayama, Y., Shibuya, T., et al., 1994. Gadolinium DTPA-enhanced magnetic resonance imaging of cerebral contusions. *Acta Neurochir. Suppl. (Wien)* 60, 472–474.
- Lezak, M.D., Howieson, D.B., Loring, D.W., 2004. *Neuropsychological assessment*, 4th ed. Oxford University Press, New York.
- Li, Y., Li, M., Zuo, L., et al., 2018. Compromised blood-brain barrier integrity is associated with total magnetic resonance imaging burden of cerebral small vessel disease. *Front. Neurol.* 9, 221.
- Lublinsky, S., Major, S., Kola, V., et al., 2019. Early blood-brain barrier dysfunction predicts neurological outcome following aneurysmal subarachnoid hemorrhage. *EBioMedicine* 43, 460–472.
- Management of Concussion/mTBI Working Group. VA/DoD Clinical Practice Guideline for Management of Concussion/Mild Traumatic Brain Injury. *J Rehabil Res Dev* 2009; 46:CP1-68.
- Mathur, M., Jones, J.R., Weinreb, J.C., 2020. Gadolinium deposition and nephrogenic systemic fibrosis: a radiologist's primer. *RadioGraphics* 40, 153–162.
- McMahon, P.J., Hricik, A., Yue, J.K., et al., 2014. Symptomatology and functional outcome in mild traumatic brain injury: results from the prospective TRACK-TBI study. *J. Neurotrauma* 31, 26–33.
- Meares, S., Shores, E.A., Taylor, A.J., et al., 2011. The prospective course of postconcussion syndrome: the role of mild traumatic brain injury. *Neuropsychology* 25, 454–465.
- Montagne, A., Barnes, S.R., Sweeney, M.D., et al., 2015. Blood-brain barrier breakdown in the aging human hippocampus. *Neuron* 85, 296–302.
- Nichols P, Urriola J, Miller S, et al. Blood-brain barrier dysfunction significantly correlates with serum matrix metalloproteinase-7 (MMP-7) following traumatic brain injury. *NeuroImage: Clinical* 2021;31:102741.
- O'Keeffe, E., Kelly, E., Liu, Y., et al., 2020. Dynamic blood-brain barrier regulation in mild traumatic brain injury. *J. Neurotrauma* 37, 347–356.
- Patlak, C.S., Blasberg, R.G., Fenstermacher, J.D., 1983. Graphical evaluation of blood-to-brain transfer constants from multiple-time uptake data. *J. Cereb. Blood Flow Metab.* 3, 1–7.
- Raja, R., Rosenberg, G.A., Caprihan, A., 2018. MRI measurements of Blood-Brain Barrier function in dementia: A review of recent studies. *Neuropharmacology* 134, 259–271.
- Reitan, R.M., Wolfson, D., Reitan, R.M., 1985. The Halstead-Reitan neuropsychological test battery: theory and clinical interpretation. Neuropsychology Press, Tucson, Ariz.
- Ripollés, P., Marco-Pallarés, J., de Diego-Balaguer, R., et al., 2012. Analysis of automated methods for spatial normalization of lesioned brains. *NeuroImage* 60, 1296–1306.
- Schweitzer, A.D., Niogi, S.N., Whitlow, C.J., et al., 2019. Traumatic brain injury: imaging patterns and complications. *RadioGraphics* 39, 1571–1595.
- Seghier, M.L., Price, C.J., 2016. Visualising inter-subject variability in fMRI using threshold-weighted overlap maps. *Sci. Rep.* 6, 20170.
- Smith, D.H., Johnson, V.E., Trojanowski, J.Q., et al., 2019. Chronic traumatic encephalopathy — confusion and controversies. *Nat. Rev. Neurol.* 15, 179–183.
- Sourbron, S.P., Buckley, D.L., 2013. Classic models for dynamic contrast-enhanced MRI: classic models for DCE-MRI. *NMR Biomed.* 26, 1004–1027.
- Tagge, C.A., Fisher, A.M., Minaeva, O.V., et al., 2018. Concussion, microvascular injury, and early tauopathy in young athletes after impact head injury and an impact concussion mouse model. *Brain* 141, 422–458.
- Tomkins, O., Feintuch, A., Benifla, M., et al., 2011. Blood-brain barrier breakdown following traumatic brain injury: A possible role in posttraumatic epilepsy. *Cardiovasc. Psychiatry Neurol.* 2011, 1–11.
- van de Haar, H.J., Jansen, J.F.A., Jeukens, C.R.L.P.N., et al., 2017. Subtle blood-brain barrier leakage rate and spatial extent: Considerations for dynamic contrast-enhanced MRI. *Med. Phys.* 44, 4112–4125.
- Veksler, R., Vazana, U., Serlin, Y., et al., 2020. Slow blood-to-brain transport underlies enduring barrier dysfunction in American football players. *Brain* 143, 1826–1842.
- Wechsler, D., 2014. Wechsler adult intelligence scale-fourth edition (WAIS-IV). Pearson, San Antonio, TX.
- Weissberg, I., Veksler, R., Kamintsky, L., et al., 2014. Imaging blood-brain barrier dysfunction in football players. *JAMA Neurol.* 71, 1453–1455.
- Winter, C., Bell, C., Whyte, T., et al., 2015. Blood-brain barrier dysfunction following traumatic brain injury: correlation of K^{trans} (DCE-MRI) and SUVR (99mTc-DTPA SPECT) but not serum S100B. *Neurol. Res.* 37, 599–606.
- Yoen, H., Yoo, R.E., Choi, S.H., et al., 2021. Blood-brain barrier disruption in mild traumatic brain injury patients with post-concussion syndrome: evaluation with region-based quantification of dynamic contrast-enhanced MR imaging parameters using automatic whole-brain segmentation. *Korean J. Radiol.* 22, 118–130.
- Yoo, R.-E., Choi, S.H., Oh, B.-M., et al., 2019. Quantitative dynamic contrast-enhanced MR imaging shows widespread blood-brain barrier disruption in mild traumatic brain injury patients with post-concussion syndrome. *Eur. Radiol.* 29, 1308–1317.
- Zlokovic, B.V., 2011. Neurovascular pathways to neurodegeneration in Alzheimer's disease and other disorders. *Nat. Rev. Neurosci.* 12, 723–738.